Research Article

NMR IN BIOMEDICINE

Received: 2 June 2010, Revised: 15 December 2010, Accepted: 16 December 2010, Published online in Wiley Online Library: 8 March 2011

(wileyonlinelibrary.com) DOI:10.1002/nbm.1675

B_0 field inhomogeneity considerations in pseudo-continuous arterial spin labeling (pCASL): effects on tagging efficiency and correction strategy

Hesamoddin Jahanian[a,b]*, Douglas C. Noll[a,b] and Luis Hernandez-Garcia[a,b]

Pseudo-continuous arterial spin labeling (pCASL) is a very powerful technique to measure cerebral perfusion, which circumvents the problems affecting other continuous arterial spin labeling schemes, such as magnetization transfer and duty cycle. However, some variability in the tagging efficiency of the pCASL technique has been reported. This article investigates the effect of B_0 field inhomogeneity on the tagging efficiency of the pCASL pulse sequence as a possible cause of this variability. Both theory and simulated data predict that the efficiency of pseudo-continuous labeling pulses can be degraded in the presence of off-resonance effects. These findings are corroborated by human *in vivo* measurements of tagging efficiency. On the basis of this theoretical framework, a method utilizing B_0 field map information is proposed to correct for the possible loss in tagging efficiency of the pCASL pulse sequence. The efficiency of the proposed correction method is evaluated using numerical simulations and *in vivo* implementation. The data show that the proposed method can effectively recover the lost tagging efficiency and signal-to-noise ratio of pCASL caused by off-resonance effects. Copyright © 2011 John Wiley & Sons, Ltd.

Keywords: cerebral blood flow; perfusion; arterial spin labeling; pCASL; tagging efficiency; labeling efficiency; off-resonance; field inhomogeneity; correction

INTRODUCTION

Perfusion is a well-known indicator of brain function. It is used to study the normal physiology and pathology of the brain (1–3). Arterial spin labeling (ASL) techniques permit the quantitative measurement of perfusion with MRI without the injection of exogenous tracers (4).

In addition to steady-state perfusion measurements, ASL is capable of estimating transient perfusion changes, which can be used to study brain function (5–7). Perfusion-based functional MRI through ASL has remarkable potential as a tool for the study of brain function because of its quantifiable nature and close relation to neuronal activity. Although it is possible to saturate the tissue of interest with tagged blood using longer radiofrequency (RF) tagging pulses (continuous arterial spin labeling, CASL) (8,9) and to improve the signal-to-noise ratio (SNR) of perfusion measurements, ASL techniques still suffer from low SNR and magnetization transfer effects, which make multislice measurements problematic.

The recent introduction of pseudo-continuous inversion pulses (pseudo-continuous arterial spin labeling, pCASL) (10,11) facilitates the use of CASL by providing multislice cerebral perfusion measurements whilst compensating for magnetization transfer effects in an efficient manner without using additional hardware or losing tagging efficiency, yet limiting the specific absorption rate (SAR). pCASL employs a rapidly repeated gradient and RF pulses to mimic the effect of continuous labeling without the need for continuous RF transmit capabilities.

However, it has been reported that the tagging efficiency of pCASL can vary greatly for different subjects, and also for different tagging locations in the same subject. These findings have been observed in 3-T (12–16), 7-T (17,18) and 11.75-T (19) ASL studies.

Any loss in the tagging efficiency of pCASL causes a loss in SNR which cannot be neglected, given the inherently low SNR of ASL. Furthermore, any unaccounted loss of tagging efficiency also results in significant quantification errors. In this article, we investigate the effects of B_0 field inhomogeneity on the efficiency of the pseudo-continuous inversion pulses as a possible cause for these variations in the tagging efficiency and propose a method to resolve this. We propose to restore the loss in tagging efficiency by correcting the phase of the RF pulses in combination with an average gradient compensation scheme. We demon-

* *Correspondence to: H. Jahanian, Functional MRI Laboratory, University of Michigan, 2360 Bonisteel Ave., Ann Arbor, MI 48109-2108, USA. E-mail: Hesam@umich.edu*

a *H. Jahanian, D. C. Noll, L. Hernandez-Garcia Functional MRI Laboratory, University of Michigan, Ann Arbor, MI, USA*

b *H. Jahanian, D. C. Noll, L. Hernandez-Garcia Department of Biomedical Engineering, University of Michigan, Ann Arbor, MI, USA*

Abbreviations used: *ASL, arterial spin labeling; CASL, continuous arterial spin labeling; pCASL, pseudo-continuous arterial spin labeling; RF, radiofrequency; SAR, specific absorption rate; SNR, signal-to-noise ratio.*

Copyright © 2011 John Wiley & Sons, Ltd.

strate the effects of field inhomogeneity and efficacy of the proposed method using numerical simulations, phantom study and *in vivo* experimental data.

THEORY

Adiabatic inversion occurs when spins experience an RF magnetic field B_1 of sweeping frequency relative to their resonance frequency (20). In the case of flow-driven inversions (e.g. CASL), the frequency sweep is achieved by the spins moving in the direction of a magnetic field gradient. In other words, the frequency of the B_1 field is constant, but the resonant frequency of the spins changes as they move in the direction of the gradient (20).

Pseudo-continuous inversion pulses produce the flow-driven adiabatic inversion effect in a piecewise manner by exciting the magnetization vector and allowing a small amount of position-dependent phase accumulation in the transverse plane between RF pulses. Assuming that the slice-selective gradient is applied along the Z direction, the phase accumulation is caused by the imbalance in the slice-selective gradient (G_{ss}) providing a net average gradient (G_{av}) between pulses. The net movement of the magnetization vector closely resembles the motion of continuous adiabatic inversions (10,11).

Let us consider a single cycle in a pseudo-continuous inversion pulse, as depicted in Fig. 1 (10,11). Ideally, for a flowing spin moving at velocity V along the Z direction, which is at distance $Z(t)$ from the iso-center, the amount of phase accumulation between the nth and $(n+1)$th RF pulses is:

$$\Delta\phi(n) = \int_{t=n\delta}^{(n+1)\delta} \gamma G_{ss}(t)Z(t)\mathrm{d}t = \int_{t=n\delta}^{(n+1)\delta} \gamma G_{ss}(t)[Z(t=n\delta)+Vt]\mathrm{d}t$$
$$= \int_{t=n\delta}^{(n+1)\delta} \gamma G_{ss}(t)[Z(t=0)+(n-1)V\delta+Vt]\mathrm{d}t = \gamma Z(t=0)G_{av}\delta$$
$$+\gamma(n-1)VG_{av}\delta^2 + \int_{t=n\delta}^{(n+1)\delta} \gamma G_{ss}(t)Vt\,\mathrm{d}t \qquad [1]$$

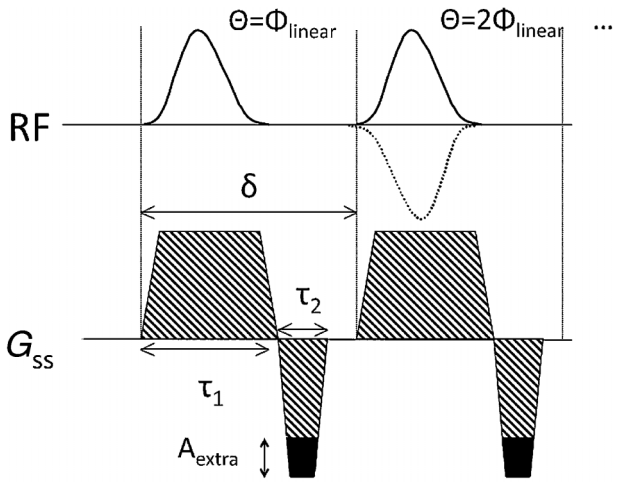

Figure 1. One cycle of the repeated pattern of radiofrequency (RF) and slice-selective gradient (G_{ss}) pulses used for pseudo-continuous inversion, where the control sequence is shown as a dotted line. θ denotes the phase of each RF pulse.

where G_{ss}, δ and G_{av} represent the slice-selective gradient (assumed to be applied along the Z direction), time interval between two RF pulses and average gradient over the time between RF pulses ($G_{av} = A_{extra}/\delta$), respectively. In this formulation, $t = 0$ represents the start of the RF pulse. The first term in Equation [1] depends on the position of the tagging plane with respect to the system iso-center. This term needs to be compensated if the tagging plane is not located at the system iso-center. Adding a linear phase to the tagging/control RF pulses can compensate for the position-dependent term in Equation [1], and makes the phase accumulation of flowing spins independent of the distance from the system iso-center.

However, the field homogeneity in the tagging plane is often perturbed by the presence of the head and/or by imperfect shimming. In particular, the air–tissue interfaces in the mouth and throat and any dental work have a profound effect. We model the local field inhomogeneities at the tagging plane of the pCASL pulse as a constant shift plus a linear Z gradient, and refer to them as the 'off-resonance' (ΔB_0) and 'off-resonance gradient' (ΔG), respectively, throughout this article. In this case, the amount of error introduced into the phase accumulation ($\Delta\phi_{error}$) between two RF pulses for the pCASL pulse sequence (Fig. 1) can be calculated using:

$$\Delta\phi_{error} = \gamma\Delta B_0\delta + \frac{1}{2}\gamma V\Delta G\delta^2 \qquad [2]$$

ΔB_0 and ΔG can be estimated from a field map collected within the tagging plane, using a first-order linear fit. As can be seen in Equation [2], ΔG induces an unwanted velocity-dependent phase in the magnetization vector during the interval between RF pulses that can degrade the adiabatic inversion. Off-resonance (ΔB_0) produces a position-dependent phase error in the magnetization vector that can further degrade the inversion.

We propose to compensate for ΔG by updating the area of the refocusing lobe of the slice-selective gradient (see Fig. 1) by ΔA_{extra}, such that:

$$\Delta A_{extra} = -\Delta G\delta \qquad [3]$$

This change will restore the change in average gradient (G_{av}) and, consequently, the frequency sweep. It also rewinds the velocity-dependent portion of $\Delta\phi_{error}$ (Equation [2]) without the need to make any assumption about the flow velocity. It should be noted that the linear phase, initially added to compensate for the position-dependent phase accumulation term (Equation [1]), also needs to be updated accordingly. The remainder of $\Delta\phi_{error}$, caused by off-resonance effects (ΔB_0), will then be compensated by adding a linear phase ϕ_{linear} to the RF pulses (Fig. 1). ϕ_{linear} can be calculated by:

$$\phi_{linear} = \gamma\Delta B_0\delta \qquad [4]$$

The application of these changes to the pulse sequence provides us with the appropriate frequency sweep and phase accumulation between two RF pulses, needed to achieve high inversion efficiency.

METHODS

Simulation

We simulated the behavior of the net magnetization vector of an ensemble of moving spins in the presence of a pseudo-continuous inversion pulse sequence using a numerical

Copyright © 2011 John Wiley & Sons, Ltd.

implementation of the Bloch equation. The step size in the simulations was 1 μs and the behavior of spins was simulated over a 500 ms window (250 ms before and 250 ms after passing the tagging plane) using 500000 data points. The spins were moving along the Z direction, perpendicular to the tagging plane. At the static magnetic field strength of 3T, T_1 and T_2 were 1664 and 250 ms, respectively (21,22). We used a 500 ms train of Hanning-window-shaped RF pulses (width, 500 μs), with 1500 μs between pulses, during a slice-selective gradient (0.6 G/cm) and followed by a refocusing gradient. We unbalanced the area of the refocusing gradient by a variable amount to achieve a net average gradient (G_{av}). In the control pulse sequence, we reversed the sign of every other RF pulse (dotted plot in Fig. 1).

The ensemble of spins moved with laminar flow in a cylinder with a radius of 0.4 cm (23). To obtain a more realistic simulation, we considered a distribution of peak velocities for laminar flow. We derived this peak velocity distribution from a model of the carotid blood flow velocity waveform suggested in ref. (24), with minimum and maximum velocities of 20 and 108 cm/s, respectively. We used the derived distribution shown in Fig. 2 for weighted averaging of the tagging efficiency calculated for each velocity to obtain the overall tagging efficiency.

The tagging efficiency (α) for each velocity was measured at the end of the pulse train (i.e. 250 ms after the spins crossed the tagging plane) using:

$$\alpha = \frac{\left|\vec{M}_{Z\text{control}} - \vec{M}_{Z\text{tag}}\right|}{2\left|\vec{M}_{Z\text{control}}\right|} \qquad [5]$$

We introduced an artifactual shift in the resonance frequency and an off-resonance gradient (ΔB_0 and ΔG) to the pulse sequence in order to simulate the field inhomogeneity effects described earlier. We corrected the effect of these errors using the proposed method.

Using the simulated pCASL sequence, we performed the following studies: (i) determination of the optimum values of G_{av} and flip angle under ideal conditions (i.e. no off-resonance or gradient distortion); (ii) investigation of the effect of field inhomogeneity on the inversion efficiency by adding artifactual off-resonance and off-resonance gradient to the simulation; and (iii) evaluation of the efficiency of the proposed method in recovering the degraded inversion efficiency.

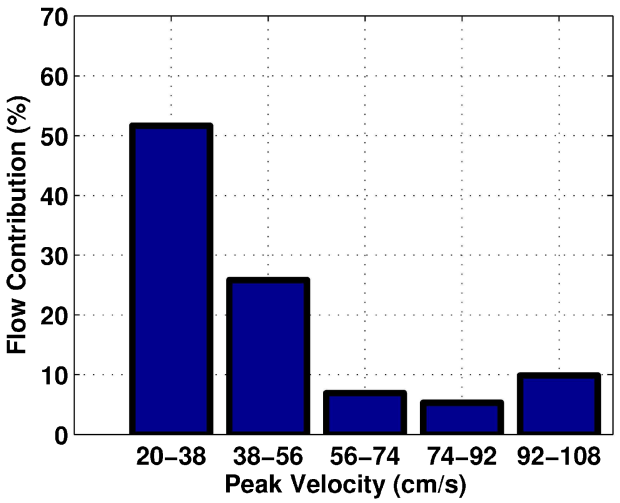

Figure 2. Contribution of different peak blood velocities to the blood flow transporting to the brain.

Phantom study

The pCASL pulse sequence shown in Fig. 1 was implemented on a 3.0-T Signa Excite scanner (General Electric, Waukesha, WI, USA). The experiment was carried out using the simulation study parameters, variable G_{av} and a flip angle of 35°. The tagging/control duration was 900 ms. Image acquisition was performed immediately after the tagging/control pulses using a gradient-echo spiral imaging sequence (TR = 1000 ms; TE = 3 ms; flip angle, 90°; number of slices, 1; slice thickness, 7 mm; field of view, 24 cm; 48 frames). We used no flow suppression gradients. We also estimated a magnetic field inhomogeneity map from two sagittal images acquired with a TE difference of 1 ms (25).

We imaged a flow phantom consisting of a polyurethane tube carrying tap water, which was recirculated with a Master-Flex LS peristaltic pump (Cole Parmer, Vernon Hills, IL, USA) with a flow velocity of 30 cm/s, using the described pCASL sequence. We located the tagging plane 3 cm below the imaging plane in the phantom. We measured the tagging efficiency within the tube of the flow phantom using Equation [5]. We measured the tagging efficiency for different values of average gradient and linear phase. We measured the tagging efficiency as a function of linear phase correction to the RF pulses (ϕ_{linear}) at several levels of the average gradient (G_{av}). The optimum parameters were compared with those predicted by the proposed technique using the off-resonance and off-resonance gradients estimated from the magnetic field inhomogeneity map. We derived the off-resonance values within the tube located inside the tagging plane (approximate thickness, 2 cm). We estimated the shift in the resonance frequency and off-resonance gradient by fitting a line to the derived off-resonance values using the least-square error-fitting technique.

In vivo experiments

Five subjects were scanned using a 3.0-T Signa Excite scanner (General Electric) in accordance with the University of Michigan's Internal Review Board regulations.

The experiment was carried out using the optimum set of pCASL pulse sequence parameters found in our simulation study (G_{av} = 0.039 G/cm; flip angle, 35°). G_{av} and ϕ_{linear} were then modified according to the proposed method (Equation [3] and Equation [4]).

Tagging/control was applied for 1800 ms, followed by a post-inversion delay of 1700 ms before image acquisition. Tagged and control images were collected alternately during 16 image acquisitions. The tagging plane was located at the carotid arteries (approximately 6 cm below the circle of Willis). Images were collected using a gradient-echo spiral imaging sequence (TR = 4000 ms; TE = 3 ms; number of slices, 9; slice thickness, 7 mm; field of view, 24 cm). We used no flow suppression gradients.

We calculated a coronal magnetic field map of the tagging region for each subject prior to the ASL study from two images acquired with a TE difference of 1 ms (25). Using the coronal field inhomogeneity maps obtained, we estimated the off-resonance and off-resonance gradient for each subject by fitting a line to the off-resonance values within each artery. We manually defined the

Copyright © 2011 John Wiley & Sons, Ltd.

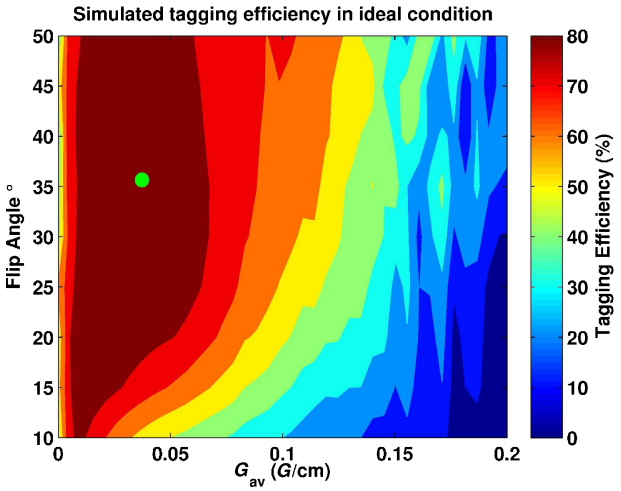

Figure 3. Simulated tagging efficiency in the ideal case for different values of flip angle and average gradient. The working point chosen for use in later studies is highlighted with a green dot.

location of the arteries on the field inhomogeneity map using the associated anatomical images. For each artery, we derived the off-resonance values within the artery located inside the tagging plane (approximate thickness, 2 cm). We estimated the shift in the resonance frequency and off-resonance gradient by fitting a line to the derived off-resonance values using a least-square error-fitting technique. Finally, we averaged the estimated values together. We performed standard shimming on the whole brain, including the tagging and imaging planes, at the beginning of each study and kept the shimming values the same for all scans, including field map estimation.

For each subject, we performed two ASL studies: (i) using the initial parameters obtained from the simulation study; and (ii) using the modified parameters suggested by the proposed method.

To evaluate the efficiency of the proposed method, for each subject, we estimated the SNR and tagging efficiency (Equation [5]) before and after correction. We acquired a high-resolution (256×256) T_1-weighted anatomical image using the same prescription as employed for ASL studies. We created a gray matter mask by segmentation of the T_1-weighted image after co-registration to the perfusion images. Using the gray matter mask, we calculated SNR as the mean gray matter signal change over the time course divided by its temporal standard deviation.

To check whether the proposed method was successful in providing the optimum tagging efficiency for each subject, we measured the tagging efficiency in the carotid arteries by tagging at approximately 6 cm below the circle of Willis and imaging one axial slice at approximately 3 cm below the circle of Willis (TR = 500 ms; tagging/control time, 400 ms; no post-inversion delay; 16-shot spiral image acquisition with 128×128 matrix; field of view, 20 cm). We measured the tagging efficiency for different ϕ_{linear} values between 0 and $-\pi$ (tagging efficiency curve) for the average gradient suggested by the proposed method and that proposed by the simulation study (Equation [3]).

RESULTS

Simulation study results

Figure 3 shows the simulated tagging efficiency for a range of flip angles and average slice-selective gradients under ideal conditions (homogeneous magnetic field). There is a broad region of G_{av} and flip angle that can provide high (i.e. $>80\%$) tagging efficiency. We chose the parameters highlighted with a green dot ($G_{av} = 0.039$ G/cm; flip angle, 35°) as the starting working point for subsequent studies. The tagging efficiency achieved at this point was 87%.

Figure 4a shows the tagging efficiency achieved using the optimal parameters obtained above, but in the presence of different amounts of off-resonance and off-resonance gradient. The negative tagging efficiencies in Fig. 4a represent the situations in which the order of tagging and control effectively changed as a result of shifts greater than π in the phase of RF pulses. We then applied the proposed correction method to recover the compromised tagging efficiencies at each point. Figure 4b shows the tagging efficiencies obtained after correction. As an example, the M_Z profile of a spin passing the pCASL tagging plane at three different situations is shown in Fig. 5: (i) ideal case without any field inhomogeneity; (ii) with field inhomogeneity ($\Delta G = -0.01$ G/cm; off-resonance, -125 Hz) before correction; and (iii) with field inhomogeneity after correction. The shift in the tagging plane from its original position as a result of off-resonance should be noted (blue relative to black curve). As can be seen, the proposed

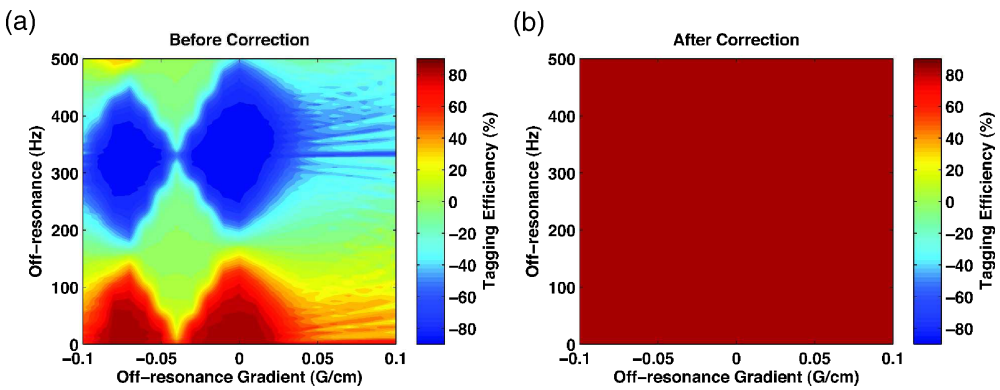

Figure 4. Simulation study results. Tagging efficiencies measured for different amounts of off-resonance and off-resonance gradient: (a) before correction; (b) after correction using the proposed method. The negative tagging efficiencies represent the situations in which the order of tagging and control changed as a result of radiofrequency (RF) pulse phase shifts greater than π.

Copyright © 2011 John Wiley & Sons, Ltd.

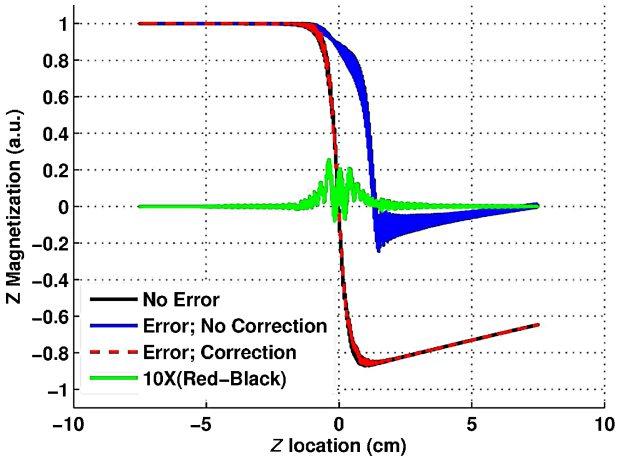

Figure 5. Simulated profile of the magnetization vector of a spin in the Z direction (Mz) passing the pseudo-continuous arterial spin labeling (pCASL) tagging plane located at $Z = 0$ cm: **black**, no field inhomogeneity; **blue**, with field inhomogeneity ($\Delta G = -0.01$ G/cm; off-resonance, -125 Hz) before correction; **red**, with field inhomogeneity after correction (note overlap between red/black). The magnified difference ($10\times$) between red and black lines is also shown (**green**).

correction method successfully restored the compromised inversion efficiencies for all amounts of off-resonance and off-resonance gradients.

Phantom study results

We measured the tagging efficiency curve for different amounts of G_{av} in a flow phantom consisting of a tube with known velocity (30 cm/s). These curves are shown in Fig. 6. The black arrow in Fig. 6 points to the starting working point suggested by the simulation study in the ideal situation (i.e. no field inhomogeneity), and the green arrow points to the modified working point suggested by the proposed method using the field inhomogeneity map information (off-resonance, 55 Hz; $\Delta G = -0.01$ G/cm at the tagging plane). As can be seen, the modification of G_{av} and addition of the linear phase (ϕ_{linear}), according to the proposed method, improved the tagging efficiency by approximately 40%.

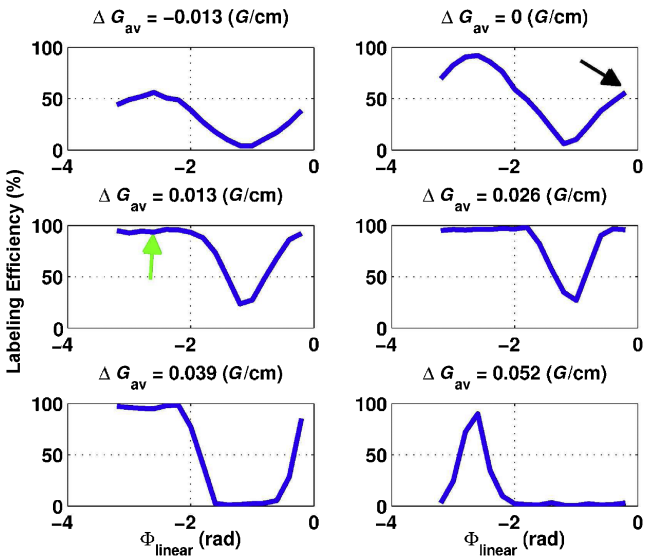

Figure 6. Tagging efficiency curves measured in a flow phantom for different average gradients. The working points suggested by numerical simulation in an ideal situation (homogeneous magnetic field) and by the proposed method (using field inhomogeneity map information) are indicated by black and green arrows, respectively.

Table 1. *In vivo* measurements of the tagging efficiency and signal-to-noise ratio (SNR) of the subtraction images before and after the proposed correction

	Subject				
	1	2	3	4	5
Tagging efficiency before correction (%)	17	62	38	79	78
Tagging efficiency after correction (%)	73	80	77.5	75	77
SNR before correction	0.18	4.26	2.88	5.98	4.80
SNR after correction	11.45	7.84	7.12	5.54	4.90

In vivo results

For each subject, the SNR and tagging efficiency were measured before and after correction using the proposed method. The measured SNRs and tagging efficiencies, together with the corresponding estimated off-resonance and off-resonance gradient, are presented in Tables 1 and 2. As can be seen, the proposed method considerably improved the SNR and tagging efficiency in subjects 1, 2 and 3. The field inhomogeneity map estimated for subject 1, which showed the greatest improvement, is given in Fig. 7. Perfusion difference images for this subject before and after correction using the proposed method are presented in Fig. 8a, b. The tagging efficiency curves of this subject are also shown in Fig. 8c, d. The black arrow points to the working point suggested by our simulation study in the ideal situation (no field inhomogeneity) and used for the acquisition of perfusion images in Fig. 8a. The green arrow points to the working point suggested by the proposed method and used for the acquisition of the perfusion image in Fig. 8b. As can be seen, the proposed method successfully recovered the degraded tagging efficiency.

DISCUSSION

The method proposed in this article is intended to compensate for the inhomogeneity of the magnetic field in the tagging region using phase-corrected RF pulses. In a sense, it can be considered as an RF shimming method for pCASL. In a situation in which there is a procedure that can provide ideal shimming in both the imaging and tagging locations, the proposed correction method will not be necessary. Our experience, however, is quite the opposite. We used standard and high-order shimming procedures on the whole brain, including the tagging and imaging planes, but our efforts were not successful and, in some cases, higher order shimming even led to further distortion of the field at the tagging or the imaging planes. Thus, in cases in which shimming is insufficient, as is the situation at higher field (> 7 T), this straightforward phase correction technique can provide the necessary tagging efficiency.

Copyright © 2011 John Wiley & Sons, Ltd.

NMR IN BIOMEDICINE

Table 2. *In vivo* measurements of the magnetic field off-resonance and off-resonance gradient at the tagging plane for different arteries

		Subject				
		1	2	3	4	5
Off-resonance (Hz)	LC	79	−120	−167	53	−88
	RC	89	−117	−166	50	−78
	LV	115	−173	−189	60	−113
	RV	160	−168	−190	55	−120
	Mean	111	−144	−178	54	−100
Off-resonance gradient (G/cm)	LC	−0.021	−0.005	0.003	0.001	0.013
	RC	−0.020	0.006	0.003	0.001	0.009
	LV	−0.004	−0.003	0.004	−0.001	0.006
	RV	−0.010	0.005	0.003	−0.001	0.017
	Mean	−0.014	0.001	0.003	0.000	0.011

LC, RC, LV and RV represent left carotid artery, right carotid artery, left vertebral artery and right vertebral artery, respectively.

In addition to modulating the average gradient and phase accumulation between RF pulses, there is another mechanism involved in the degradation of the tagging efficiency as a result of a shift in the resonance frequency. Off-resonance shifts the spatial location of the tagging plane. It also shifts the frequency sweep profile. However, as G_{av} is much smaller than G_{max} (0.039 *versus* 0.6 G/cm in this study), a shift in resonance frequency shifts the tagging slab slightly, but shifts the frequency sweep much more (see Fig. 5 and note the shift in the blue relative to the black curve). The mismatch between the RF pulse profile and the frequency sweep profile can lead to further degradation of the tagging efficiency. By applying the proposed corrections, in addition to correcting the frequency sweep and phase accumulation, we also shift the frequency sweep back to the intended location.

An orientation offset between an artery and the applied gradient direction will change the effective velocity of the blood

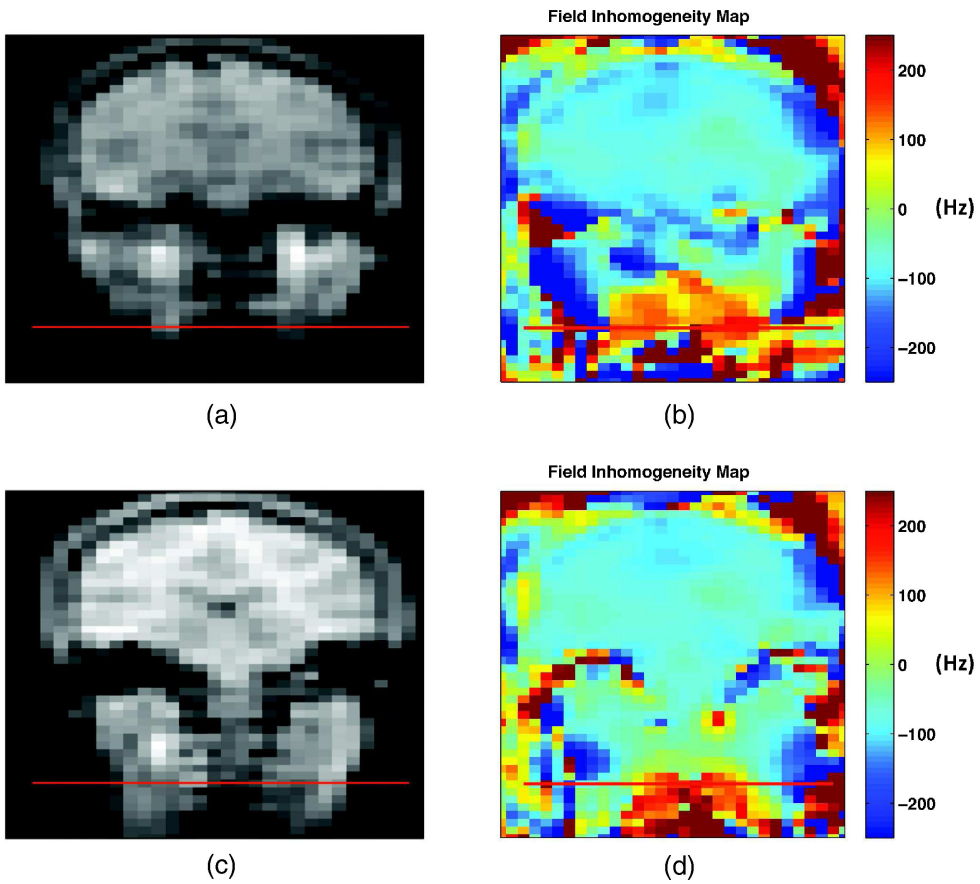

Figure 7. Estimated field inhomogeneity map for subject 1. The location of the tagging plane is shown by the red line in the photographs. (a, b) The anatomical image and corresponding field inhomogeneity map at the level of the carotid arteries. (c, d) The anatomical image and corresponding field inhomogeneity map at the level of the vertebral arteries.

Copyright © 2011 John Wiley & Sons, Ltd.

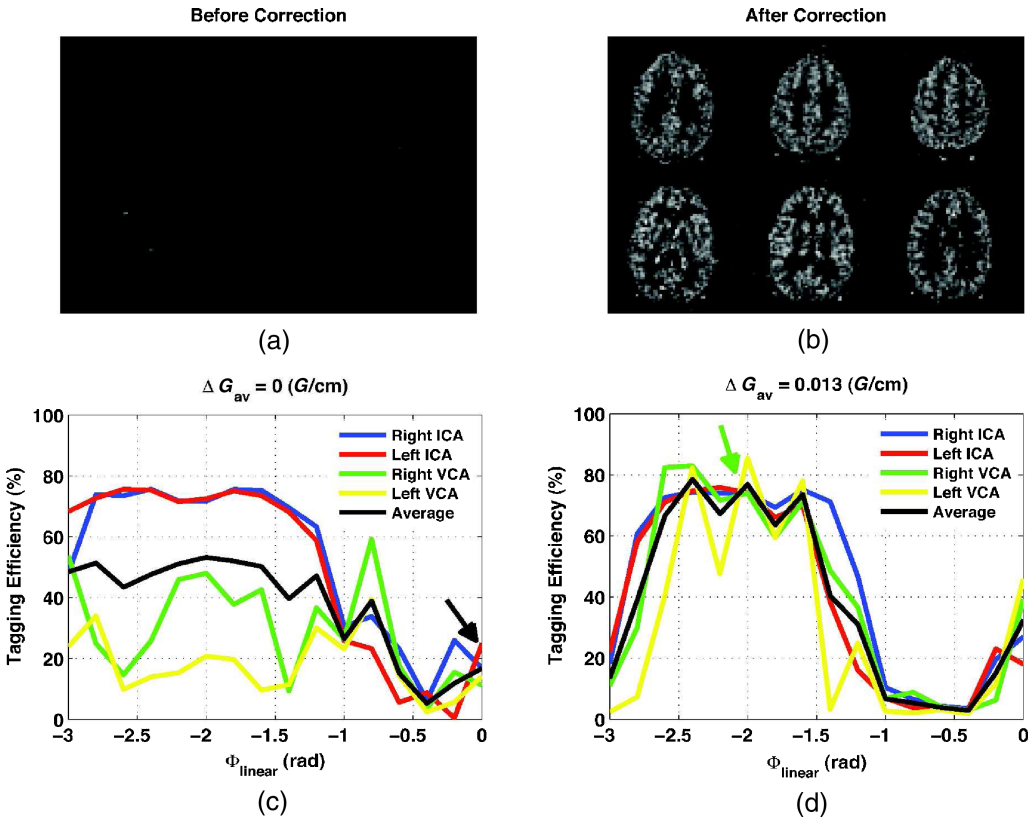

Figure 8. Perfusion difference images for subject 1 acquired before (a) and after (b) correction using the proposed method. Tagging efficiency curves measured in the left and right internal carotid arteries (ICA) and vertebral arteries (VCA) before (c) and after (d) correction for the off-resonance gradient (δ) in the same subject. The black and green arrows point to the working points suggested by the simulation study and the proposed method, respectively.

spins along the gradient direction, which can change the phase accumulation of spins between RF pulses depending on the angle between the artery and gradient direction. In addition, the presence of a through plane gradient in this situation will further modulate the phase accumulation and can degrade the tagging efficiency. Therefore, in practice, it is better to place the tagging plane in an area in which the arteries are aligned with the applied gradient direction as much as possible.

As it is not possible to find the optimum parameters in the ideal situation (i.e. no field inhomogeneity) using experimental data, we used numerical simulation of the Bloch equation to find the starting working point. In order to make our simulations as realistic as possible, we considered a laminar blood flow with a distribution of velocities derived from the measured mean blood flow waveform suggested in ref. (24), instead of assuming plug flow, as in previous studies (11). In pulsatile blood flow of arteries, there is also an acceleration pattern, which can further change the amount of phase accumulation between RF pulses. However, given the fact that the blood velocity is fairly high in the arteries and the tagging plane is relatively narrow (~2 cm), we only considered the distribution of blood velocity in the pulsatile flow of arteries and neglected the effect of the acceleration of blood within the tagging plane. The simulated ranges of off-resonance and off-resonance gradient are wider than those observed in our results (Table 2) because we did not intentionally place our tagging plane on areas with high off-resonance and gradient errors. However, on a given field inhomogeneity map, it is possible to find areas with off-resonance and off-resonance gradient as high as those in our simulated study.

On inspection of the tagging efficiency curves of our phantom study (Fig. 6), it is apparent that it is possible to achieve a high tagging efficiency only by adding an appropriate linear phase alone for a wide range of average gradients. In that case, Equation [2] should be used to estimate the appropriate linear phase instead of Equation [4], which requires a knowledge (or an assumption) of the blood velocity. In addition, the blood flow velocity at the carotids is higher than the flow velocity of our flow phantom (30 cm/s) and, as a result, we expect the correction to be more sensitive to the choice of G_{av} in human studies. In addition, as can be seen in Fig. 4a, having an appropriate average gradient makes the pCASL pulse sequence less sensitive to the selection of the linear phase (i.e. more robustness to the errors in estimation of the appropriate linear phase).

In our subjects, the mean off-resonance and off-resonance gradient values worked well for all of the arteries. However, this might not be the case in all subjects. If the off-resonance values at the arteries are very different, it might not be possible to find a correction value that works for all of them. It that case, the difference in off-resonance between arteries can be eliminated by adding a small in-plane gradient similar to that proposed in ref. (26).

We note that, without this correction applied to the dataset presented in this article, two of the five subjects would still have yielded accurate perfusion maps with reasonable SNR. However, in two subjects, we would have been faced with considerably

Copyright © 2011 John Wiley & Sons, Ltd.

lower tagging efficiencies and SNR maps. In these cases, the quantification of perfusion maps, without the measurement of the tagging efficiencies, would have resulted in significant errors. For one of the subjects, the perfusion measurement was simply not possible without the proposed correction method.

CONCLUSION

This study shows that, even if the pCASL sequence has been theoretically optimized, the tagging efficiency of pCASL can be compromised by local shifts in the magnetic field, and thus the resonance frequency, at the tagging plane. A loss in tagging efficiency leads to lower signal-to-noise perfusion maps and can also cause considerable quantification errors if unaccounted for.

Our preliminary results show that the estimation of these field inhomogeneities using B_0 field map information and compensation using the proposed method can effectively recover the compromised tagging efficiency. This may allow the use of pCASL in a wider range of conditions (clinical or research), including high-field scanning, where it may have otherwise been impractical.

Acknowledgements

The authors thank Dr Jon-Friedrik Nielsen for helpful discussions and comments. This works was supported by the National Institutes of Health (RO1 EB004346 and R21 DA026077).

REFERENCES

1. Huang CR. Voxel- and VOI-based analysis of SPECT CBF in relation to clinical and psychological heterogeneity of mild cognitive impairment. Neuroimage, 2003; 19(3): 1137–1144.
2. Farr TD, Wegener S. Use of magnetic resonance imaging to predict outcome after stroke: a review of experimental and clinical evidence. J. Cereb. Blood Flow Metab. 2010; 30(4): 703–717.
3. Alsop DC. Assessment of cerebral blood flow in Alzheimer's disease by spin-labeled magnetic resonance imaging. Ann. Neurol. 2000; 47(1): 93–100.
4. Williams DS, Detre JA, Leigh JS, Koretsky AP. Magnetic resonance imaging of perfusion using spin inversion of arterial water. Proc. Natl. Acad. Sci. USA, 1992; 89(1): 212–216.
5. Seong-Gi K. Quantification of relative cerebral blood flow change by flow-sensitive alternating inversion recovery (FAIR) technique: application to functional mapping. Magn. Reson. Med. 1995; 34(3): 293–301.
6. Hernandez-Garcia L, Lee GR, Vazquez AL, Noll DC. Fast, pseudo-continuous arterial spin labeling for functional imaging using a two-coil system. Magn. Reson. Med. 2004; 51(3): 577–585.
7. Liu TT, Wong EC, Frank LR, Buxton RB. Analysis and design of perfusion-based event-related fMRI experiments. Neuroimage, 2002; 16(1): 269–282.
8. Alsop DC, Detre JA. Multisection cerebral blood flow MR imaging with continuous arterial spin labeling. Radiology, 1998; 208(2): 410–416.
9. Wong EC, Buxton RB, Frank LR. A theoretical and experimental comparison of continuous and pulsed arterial spin labeling techniques for quantitative perfusion imaging. Magn. Reson. Med. 1998; 40: 348–355.
10. Dai W, Garcia D, de Bazelaire C, Alsop DC. Continuous flow-driven inversion for arterial spin labeling using pulsed radio frequency and gradient fields. Magn. Reson. Med. 2008; 60(6): 1488–1497.
11. Wu WC, Fernandez-Seara M, Detre JA, Wehrli FW, Wang J. A theoretical and experimental investigation of the tagging efficiency of pseudo-continuous arterial spin labeling. Magn. Reson. Med. 2007; 58(5): 1020–1027.
12. Jahanian H, Hernandez-Garcia L, Noll DC. Correcting for off-resonance induced degradation of inversion efficiency in pseudo-continuous ASL. *Proceedings of the 17th Annual Meeting ISMRM*, Honolulu, HI, USA, 2009; 1518.
13. Jung Y, Wong EC, Liu TT. Multi-phase pseudo-continuous arterial spin labeling (MP PCASL): robust PCASL method for CBF quantification. *Proceedings of the 17th Annual Meeting ISMRM*, Honolulu, HI, USA, 2009; 622.
14. Aslan S, Xu F, Wang PL, Uh J, Yezhuvath U, Osch MV, Lu H. Labeling efficiency is critical in pseudo-continuous ASL. *Proceedings of the 17th Annual Meeting ISMRM*, Honolulu, HI, USA, 2009; 621.
15. Shin DD, Jung Y, Shankaranarayanan A, Restom K, Guo J, Lu WM, Bandettini PA, Wong EC, Liu TT. Semi-automated correction of phase errors in optimized pseudo-continuous arterial spin labeling. *Proceedings of the 18th Annual Meeting ISMRM*, Stockholm, Sweden, 2010; 1744.
16. Jahanian H, Noll DC, Hernandez-Garcia L. Optimizing the inversion efficiency of pseudo-continuous ASL pulse sequence using B0 field map information. *Proceedings of the 18th Annual Meeting ISMRM*, Stockholm, Sweden, 2010; 519.
17. Luh WM, Talagala SL, Bandettini PA. Robust prescan for pseudo-continuous arterial spin labeling at 7T: estimation and correction for off-resonance effects. *Proceedings of the 18th Annual Meeting ISMRM*, Stockholm, Sweden, 2010; 520.
18. Teeuwisse WM, Webb A, van Osch MJ. Whole brain pseudo continuous ASL at 7T using a single coil for imaging and labeling. *Proceedings of the 18th Annual Meeting ISMRM*, Stockholm, Sweden, 2010; 518.
19. Duhamel G, Callot V, Cozzone PJ, Kober F. Practical investigation of pseudo-continuous arterial spin labeling (pCASL) feasibility at very high field (11.75T). *Proceedings of the 18th Annual Meeting ISMRM*, Stockholm, Sweden, 2010; 1738.
20. Dixon WT, Du LN, Faul DD, Gado M, Rossnick S. Projection angiograms of blood labeled by adiabatic fast passage. Magn. Reson. Med. 1986; 3: 454–462.
21. Lu H, Clingman C, Golay X, van Zijl PC. Determining the longitudinal relaxation time (T1) of blood at 3.0 Tesla. Magn. Reson. Med. 2004; 52(3): 679–682.
22. Wright GA, Hu BS, Macovski A. Estimating oxygen saturation of blood in vivo with MR imaging at 1.5T. J. Magn. Reson. Imaging, 1991; 1: 275–283.
23. Arndt JO, Klauske J, Mersch F. The diameter of the intact carotid artery in man and its change with pulse pressure. Pflugers Arch. Gesamte Physiol. Menschen Tiere, 1968; 301(3): 230–240.
24. Holdsworth DW. Characterization of common carotid artery blood-flow waveforms in normal human subjects. Physiol. Meas. 1999; 20(3): 219–240.
25. Yip CY, Fessler JA, Noll DC. Advanced three-dimensional tailored RF pulse for signal recovery in $T2^*$-weighted functional magnetic resonance imaging. Magn. Reson. Med. 2006; 56(5): 1050–1059.
26. Wong EC. Vessel-encoded arterial spin-labeling using pseudocontinuous tagging. Magn. Reson. Med. 2007; 58: 1086–1091.

Copyright © 2011 John Wiley & Sons, Ltd.